

# Optimization and Investigation of Rapid Sealing Technology Based on Mine Disaster Period

Feng Li, Yadong Jing \*, Chenchen Wang, Baorui Ren, Chenyu Zhang and Guanghao Wang

School of Emergency Management and Safety Engineering, China University of Mining and Technology (Beijing), Beijing 100083, China; lifeng@cumtb.edu.cn (F.L.); bq2110102010@student.cumtb.edu.cn (C.W.); zqt2110102054@student.cumtb.edu.cn (B.R.); zhangchenyu@student.cumtb.edu.cn (C.Z.); zqt2010102037@student.cumtb.edu.cn (G.W.)

\* Correspondence: yadongjing@student.cumtb.edu.cn

**Abstract:** Due to the particularity of mine spaces and the limitations of underground ventilation, the gas in disaster areas changes greatly after a fire occurs. Rapid sealing technology is beneficial for preventing the development of fires and gas explosions by controlling oxygen. Using the Fuzzy Analytic Hierarchy Process (FAHP), in this research, we analyzed the three most effective rapid sealing processes, conducted experimental research on the three sealing processes, and developed a further optimized design. At the same time, according to different stages of blasting damage, the change characteristics and migration laws of explosive hazardous gases in a disaster area were analyzed using fluent numerical simulation. Additionally, the ability of the three optimal processes to create an airtight area was measured in this research. The applicable scenarios and scope of the three technologies were found, which provides a wider range of application scenarios and more diverse options for rapid airtightness during catastrophic periods, mine fire prevention, and explosion protection.

**Keywords:** mine fire; rapid sealing; gas disasters; gas fluctuations; process optimization



**Citation:** Li, F.; Jing, Y.; Wang, C.; Ren, B.; Zhang, C.; Wang, G. Optimization and Investigation of Rapid Sealing Technology Based on Mine Disaster Period. *Fire* **2023**, *6*, 378. <https://doi.org/10.3390/fire6100378>

Academic Editor: Thomas H. Fletcher

Received: 11 September 2023

Revised: 28 September 2023

Accepted: 29 September 2023

Published: 4 October 2023



**Copyright:** © 2023 by the authors. Licensee MDPI, Basel, Switzerland. This article is an open access article distributed under the terms and conditions of the Creative Commons Attribution (CC BY) license (<https://creativecommons.org/licenses/by/4.0/>).

## 1. Introduction

During the coal mining process, there are a variety of safety risks and accident hazards. In the field of coal mining, fire accidents are one of the five major disasters, and their negative impacts are serious and prominent. Because of the particularity of mine spaces and the limitations of underground ventilation conditions, the gas in a disaster area changes significantly after a fire occurs, and the wind speed in local areas decreases. Gas will continue to gush out from the coal wall and goaf, accumulating easily locally and reaching high concentrations or even exceeding limits, which can lead to significant safety hazards [1–3]. When conducting fire rescue underground, if the fire cannot be directly extinguished within 1–2 h of development, there is a risk of gas explosion in the disaster area with sufficient oxygen. From this perspective, it is necessary to quickly and effectively establish underground enclosed facilities to isolate the disaster area and reduce oxygen supply to prevent further expansion of the disaster [4–7]. Thus, rapid sealing technology is a practical disaster relief technology that can be used in disaster areas to effectively control the oxygen supply in fire areas.

The rapid development of mine sealing technology has led to the emergence of a large number of sealing processes and methods. The common ones are roughly divided into wooden board-and-brick airtight wall sealing, airbag-type sealing, and high-water-content-material sealing. In addition, there are a few other methods, such as closed doors, hanging net spraying, and parachute sealing [8–11]. From the perspective of materials research, Rockwell is superior to traditional materials as a filling material in terms of airtightness and construction speed of the sealing wall [12]. The reliability of the sealing effect of a closed wall was verified using a rapid solidification material, powdered coal slurry [13]. For

common airbag sealing schemes, Ma et al. [14] proposed two structural designs: flat airbags and assembled airbags. Song et al. [15] further optimized a sealed explosion-proof outer bag material and proposed an airbag-type fast sealing process to achieve long-distance, remote inflation of airbags. Meanwhile, hydrogel sealing research has mainly focused on material mechanical properties and material ratio [16,17], and has also made some progress in the transportation and filling of gel materials [18–20].

With the continuous emergence of new sealing processes and technologies, the advantages and disadvantages of various processes are obvious. At present, the most common means of achieving rapid airtightness in disaster areas are still traditional airtight methods using materials such as wooden boards and brick–concrete mixes. When rescue teams stay in a fire scene for a long time, where the risk of airtightness is relatively high, the quality and airtightness of the emergency airtight measures cause some concern. Therefore, based on the Fuzzy Analytic Hierarchy Process (FAHP), we mainly analyzed the three most effective rapid sealing processes among many processes, conducted experimental research on the three sealing processes, and developed an optimized design. At the same time, based on the Kailuan experimental tunnel in Tangshan City, Hebei Province, China, and different fire development stages, fluent numerical simulation software was used to analyze the safety of the sealing effects of the three sealing processes.

## 2. Fuzzy Decision Selection for Closed Process

In terms of comparing and contrasting the advantages and disadvantages of various sealing processes and materials, at this stage of this research, we preliminarily selected and eliminated the sealing process schemes with obvious disadvantages through investigation and research, and finally, nine sealing processes were selected for secondary optimization, namely, “sea capacity grouting, air bag sealing, high water rapid setting, hydrogel, foam concrete, fly ash, organic materials, parachute sealing, and concrete rockxiu”. The Fuzzy Analytic Hierarchy Process (FAHP) [21,22] was used to analyze the difficulty and effectiveness of various types of enclosed walls, establish a fuzzy evaluation matrix for fuzzy decision making, and select the centralized optimal plan for subsequent design and optimization.

According to reference [23], a fuzzy decision-making model was first established. The influencing weight factors determined using the Analytic Hierarchy Process (AHP) based on investigation and expert opinions are shown in Table 1. The weight of each factor compared to the previous level was calculated using the geometric average method, and then normalized to obtain

**Table 1.** Factors affecting the evaluation of rapid closure techniques.

Optimal solution	Construction difficulty factors	Front layout requires manpower Manpower required for post layout Step complexity Step controllability Construction speed
	Sealing effect factors	Tightness High-temperature resistance Construction effect Maintenance time

$W(V_1) = 0.75, W(V_2) = 0.25, B1 = (0.042, 0.33, 0.110, 0.188, 0.33), B2 = (0.587, 0.072, 0.218, 0.123).$

Additionally, the following equation was used for verification:  $CR = CI/RI, CI = (\lambda_{max} - N) / (n - 1).$

For the B1 matrix, the maximum eigenvalue is 5.023,  $CI = 0.006, RI = 1.11,$  and  $CR = 0.005 < 0.1,$  and the consistency test result is passed. For the B2 matrix, the maximum

eigenvalue is 4.019,  $CI = 0.006$ ,  $RI = 0.882$ , and  $CR = 0.007 < 0.1$ , and the consistency test result is passed.

The weights of each factor obtained are

$B = [W(V_1) \times B1, W(V_2) \times B2] = (0.0315, 0.2475, 0.0825, 0.141, 0.2475, 0.1468, 0.018, 0.0545, 0.0307)$

Finally, the fuzzy judgment matrix  $R$  was obtained, and based on the weight allocation vector and the fuzzy evaluation matrix, the weighted average model was used to calculate the following:

$A = B \times R = (0.553, 0.680, 0.648, 0.707, 0.542, 0.641, 0.611, 0.767, 0.532)$

According to the principle of maximum degree of membership, the best schemes are the scheme of air bag sealing, hydrogel, and sea capacity module grouting.

### 3. Closed Process Experiment

#### 3.1. Airbag Sealing Process

The sealing speed of an air bag is fast. After the bag is inflated, it is in tight contact with the rock wall of the tunnel and has good air tightness. An air bag can completely block a tunnel within 5 min, and the air leakage rate is controlled to within 5%, which can prevent disasters. Regional wind and smoke flow is effectively and quickly isolated. At present, when an airtight airbag is in use, rescuers still need to enter the blocked area for deployment. In order to achieve unmanned deployment, starting from the mechanical structure, we designed an airbag device that can be remotely controlled after being pre-arranged. The supporting air circuit scheme was designed to improve the reliability of the device, continuously replenish the airbag to maintain air pressure, and ensure the airbag is sealed. This design provides a new choice for airbag sealing technology [24,25].

Based on mechanical design and pneumatic circuit design, the existing airbag sealing process was optimized, and the PLC control method and remote control means were used to assist the completion. As for the practical usage, key roadway positions were pre-selected and airbag electronic control boxes were installed in advance to achieve unmanned operation of the remotely controlled airbag. A pneumatic circuit was designed for stage air supply and stable pressure to achieve stable airbag pressure, and the final airbag sealing process design was completed.

As shown in Figure 1a, this research adopts a remote-controlled fast-sealing multi-layer air bag suitable for mining tunnels, which consisted of a main airbag, a cement baffle semi-open storage box, an air tent, a pump box reserve tank, and a high-pressure gas pipe and electric control line. By utilizing the inherent properties of the airbag and remote control, the overall sealing of the tunnel can be achieved, as performed in a storage box in a safe environment, as shown in Figure 1b, achieving convenience and safety.

Figure 1c shows the air bag blocking process. The PLC control system is used to realize air bag inflation in three ways, and remote control is used to achieve unmanned operation in the tunnel. The proposed air bag sealing optimization process can quickly seal an air bag in mine accidents. The remote control mechanism enhances the airtightness, and the sealing speed is fast. It controls the direction of air flow in the tunnel, reduces the possibility of the mine rescue team members being exposed to the accident scene, and provides a new solution for the rescue team to respond quickly to achieve airtightness.

#### 3.2. Water-Absorbing Gel Process

As a high-water-content-material sealing process, gel can be used in place of a lot of sealing materials when the water source is sufficient, and an airtight structure can be built relatively quickly after the structure is reasonably designed. However, in actual application, gel sealing still has problems, such as the difficulty in attaching the capsule to the top, easy collapse, and bag body bursting under pressure. Thus, the usage of water-absorbent resin gel particles as a filler material is a choice that reduces the complexity of the operation and increases the adaptability of the process.

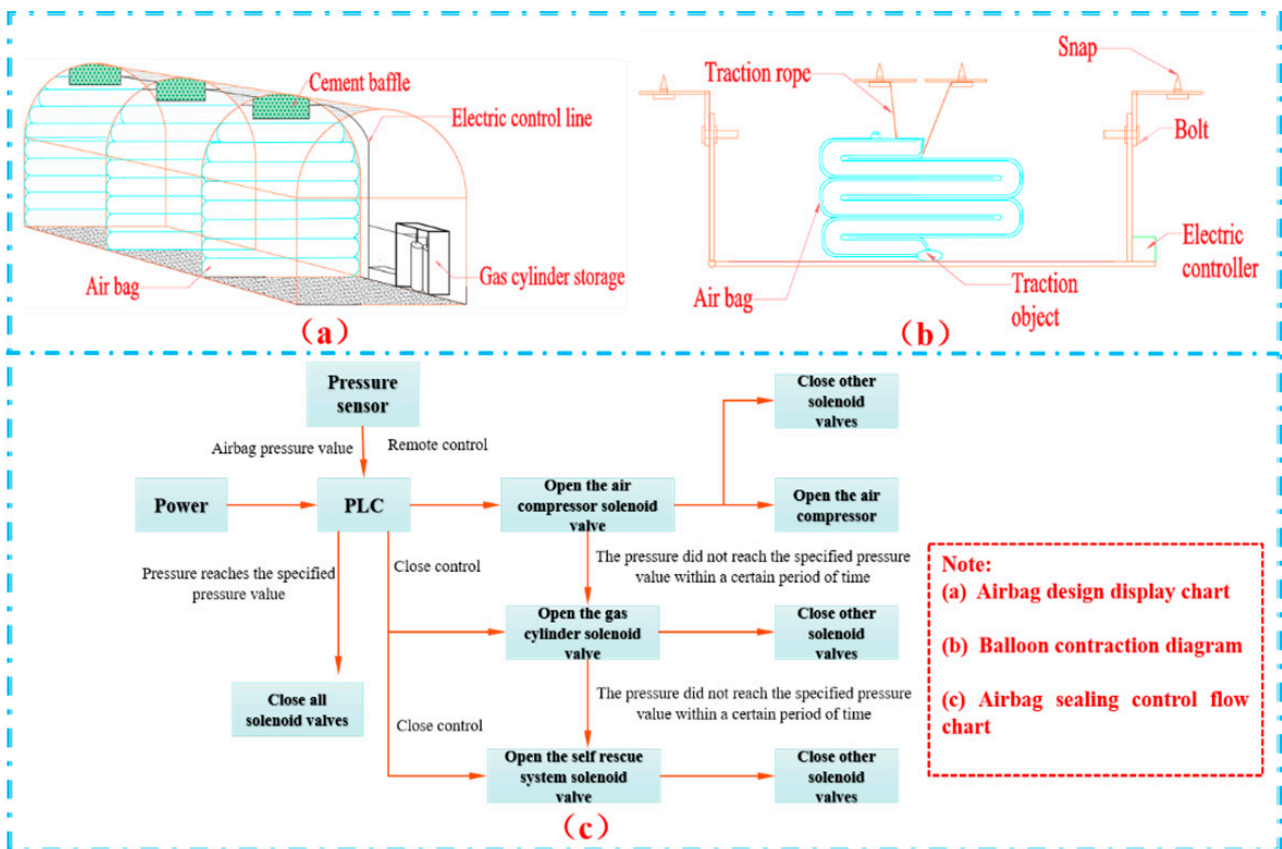


Figure 1. Airbag design diagram. (a) Airbag design display chart; (b) Balloon contraction diagram; (c) Airbag sealing control flow chart.

### 3.2.1. Laboratory Property Test of Water-Absorbing Gel

As shown in Figure 2, in order to test the water-filled expansion effect of gel and verify the vertical extension state of the hoisted gel bag, the gel particles were tested by measuring cup expansion and extension. A total of 4 g of gel particles was placed at the bottom of the measuring cup. As shown in Figure 2a,b, the gel had a good water absorption effect and fast extension speed. After absorbing water, it could expand by more than 70 times its size and quickly extend to the top of the measuring cup, with good longitudinal ductility. Through Figure 2c, it can be clearly seen that the gel had a certain plasticity after forming, and the shape remained good.

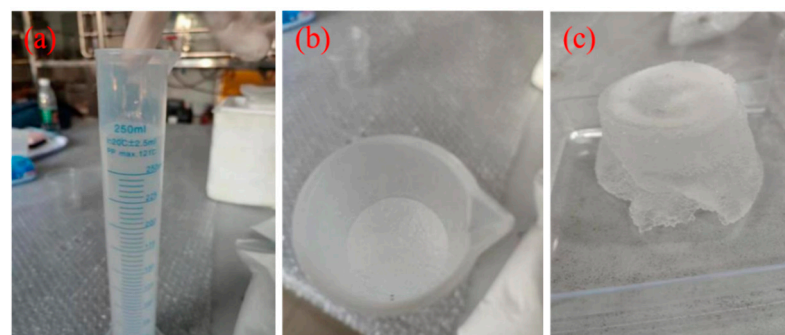
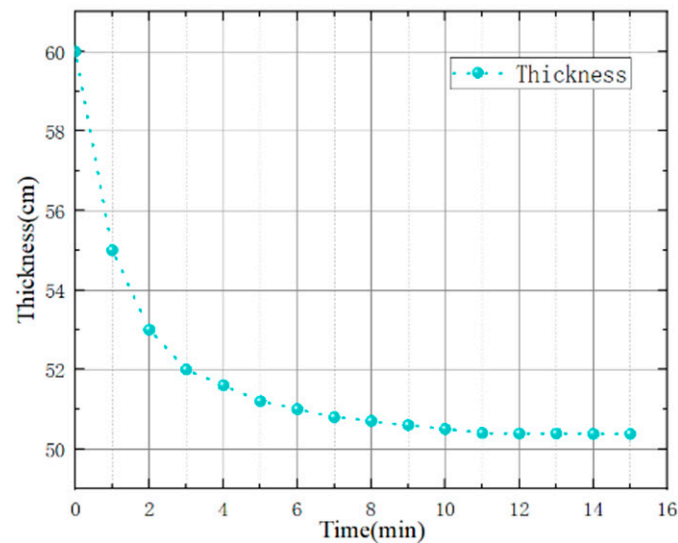


Figure 2. Gel measuring cup experiment.

As shown in Figure 3, the gel bag was compressed, gel leaked out of the bag, and the thickness of the five-layer stacked gel bags started to change with time. After 10 min, the

thickness basically had not changed, and the leaked gel could help fill the gap between the outer bag and the inner bag, which greatly promotes airtightness.



**Figure 3.** Gel bag thickness versus time diagram.

### 3.2.2. Similarity Test of Gel Capsule

In order to verify the problem of top connection, similar experiments were carried out for the design of dome-shaped outer bags. The placement method involves hoisting and arranging three gel bags at the upper end and placing two layers horizontally at the lower end, fully filled. According to the shape of the arched tunnel wall, a 5:1 EPS model was customized to prepare for the laboratory roof connection experiment using small gel bags. The outer bag was replaced with a transparent PE high-pressure flat bag for simulation, as shown in Figure 4.

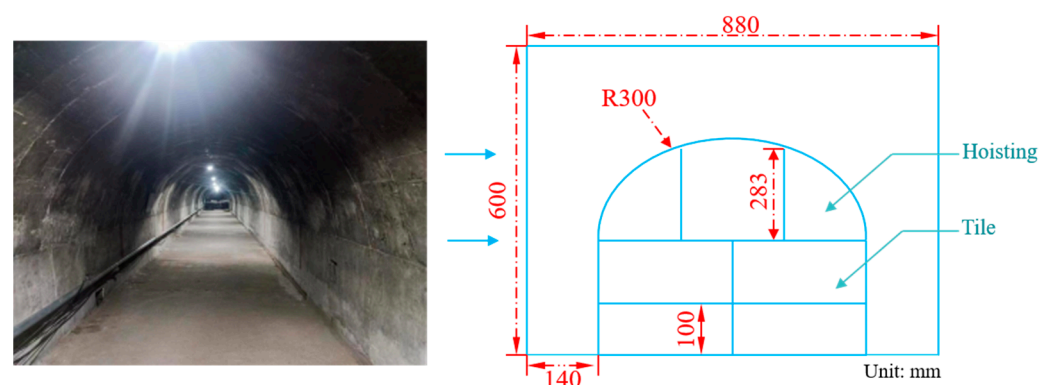


**Figure 4.** Design of similar experimental model.

Figure 5a,b reflect the arrangement and state of the gel before sealing the tunnel from different angles. The gel bag could fully fill the tunnel entrance after a certain period of time; as shown in Figure 5c, the tunnel was fully and tightly sealed, and the experimental effect was good. In this experiment, it was found that achieving a better expansion effect requires paying more attention to the speed of water injection. To facilitate the gel's absorption of water and ensure a better fit with the tunnel wall, it is recommended easily de-formable and water-permeable materials be used for the inner bag material. Therefore, sufficient water sources are needed, and the sealing speed is fast. However, personnel do not need to be on site and can be evacuated in advance.



**Figure 5.** Tunnel closing similarity model experiment.

### 3.3. Marine Capacity Module Process

As shown in Figure 6, the sea capacity module was used as the skeleton of the closed wall, into which cement was poured to form a modular cement closed structure, which not only meets the requirements of construction speed but also ensures the robustness of the closed wall itself. The characteristics of foam material make it easy to cut and adapt to different roadway shapes. In addition, in order to design the process steps and facilitate the development of a rapid sealing plan for disaster areas, it is necessary to design modular arrangements for different tunnel shapes.



**Figure 6.** Application of sea capacity module.

#### 3.3.1. Experiment on the Expansion Effect of Filling Cement

As shown in Figure 7, the laboratory chose to use expansion agents such as EP-2, FQY, HEA, SYK, HCSA, UEA, etc., to mix with grouting cement, Portland cement, and sulfoaluminate cement in a cement ratio of 8% to observe the expansion effect. Compared with the unadded samples of three types of cement, it was found that there were significant differences in the cross-section after solidification. After the expansion agents EP-2, HEA, and FQY and cement were mixed and solidified, many pores appeared inside the cement after solidification, but it did not have a significant expansion advantage compared with the original cement; as shown in Table 2, the expansion effect of each mixed sample was not significant, and the overall cement expansion rate remained below 2%.

The reason for the poor expansion effect is that the three types of cement used in the expansion agent are quick-drying cements. The initial setting of quick-drying cement occurs within 20 min, and the setting time is too short. The expansion agent will react in the early hydration stage, leading to ineffective expansion in the early stage and loss of expansion energy. In addition, cement-based materials often require high-water-content cement to achieve a certain degree of fluidity, which leads to the expansion agent being in a high-humidity environment. The expansion agent will react with water and hydration products, which can also lead to loss of expansion energy. At the later stage of hydration and during cement solidification, the expansion effect of the expansion agent is very weak, and thus does not work properly.

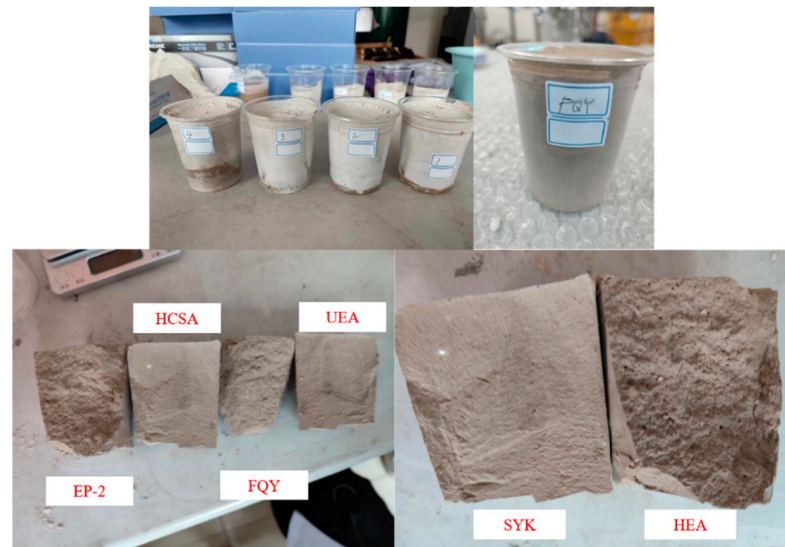


Figure 7. Laboratory proportioning experiment diagram.

Table 2. Expansion effect of expansion agent combined with non-shrinkage cement.

Type of Filler	Swelling Effect						Comparative Sample
	EP-2	FQY	HEA	SYK	HCSA	UEA	
Double-fast sulphoaluminate cement	1.00%	2.00%	1.00%	Not obvious	Not obvious	Not obvious	No shrinkage
Portland expansion cement	Not obvious	Not obvious	Not obvious	Not obvious	Not obvious	Not obvious	1.7% (three days)
Non-shrinkage grouting quick-drying cement	Not obvious	Not obvious	1.00%	Not obvious	Not obvious	Not obvious	0.3% (quick drying)

The selection of the internal filling material for the sea capacity module sealing solution involved considering the following. Firstly, it was observed that the expansion effect did not improve after adding an expansion agent. Secondly, to prevent internal cracking of the cement, the solution of using an expansion agent with more pores in the cross-section of the cement was eliminated. As a result, an experimental sample with a neat cement profile and a simple and stable formula was chosen as the filling material. Specifically, a high-strength non-shrinkage grouting cement solution without an expansion agent was selected as the internal filling material for the sea capacity module sealing solution.

### 3.3.2. Layout Design of Sea Capacity Module Tunnels

According to the shape of the experimental roadway, the arrangement of the sea capacity modules was pre-designed and the cut size of the sea capacity modules was estimated to prepare for field experiments and applications. Figure 8 is a real-life photo of the experimental tunnel, which is divided into arched tunnels and trapezoidal tunnels. As shown in Figure 9, the sea capacity module cutting arrangement design was carried out for trapezoidal and circular arch tunnels, respectively.

Through experimental optimization, non-shrinkage grouting double-fast cement was ultimately selected as the filling material for the sea capacity module scheme. A sea capacity module cutting mode was proposed for trapezoidal and circular arch tunnels to achieve rapid sealing, which has strong adaptability. However, due to the long solidification time of cement, the sealing time is longer.



Figure 8. Gallery photo.

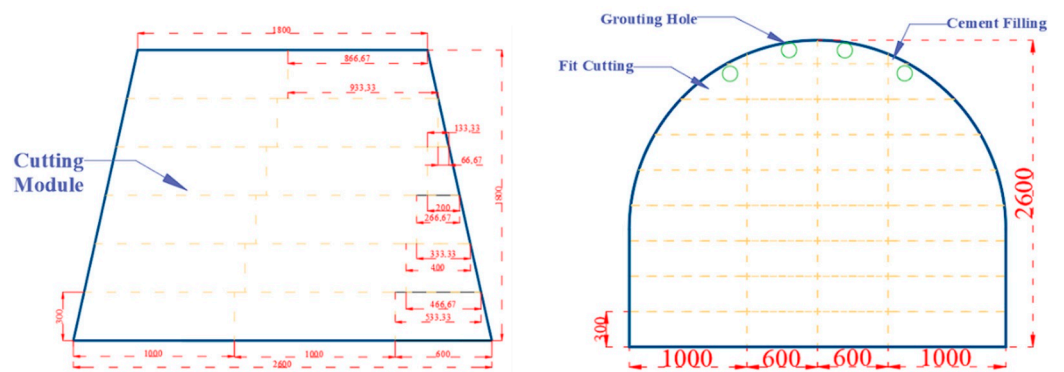


Figure 9. Cutting style of tunnel sea capacity module.

#### 4. Simulation Study on the Effectiveness of Optimization Schemes

##### 4.1. Model Establishment

Based on the experimental research and optimization of the three closed processes mentioned earlier, a simulation study was conducted to evaluate the safety of the three optimization schemes based on the speed of the three process optimizations.

In this research, we simulated a fire in a working face roadway, as shown in Figure 10, which was located on the side of the central axis of the roadway of the working face near the air duct. It is assumed that when oxygen and gas meet the conditions, the fire source position can cause a gas explosion at any time [26,27]. We used the Kailuan experimental tunnel in Tangshan as a modeling reference. After simplifying the complex working conditions, the coal mine working face ventilation volume and gas emission data were used to simulate the migration of catastrophic gases in the underground tunnel before and after sealing, and the simulation results for the explosion hazard areas were analyzed and identified.

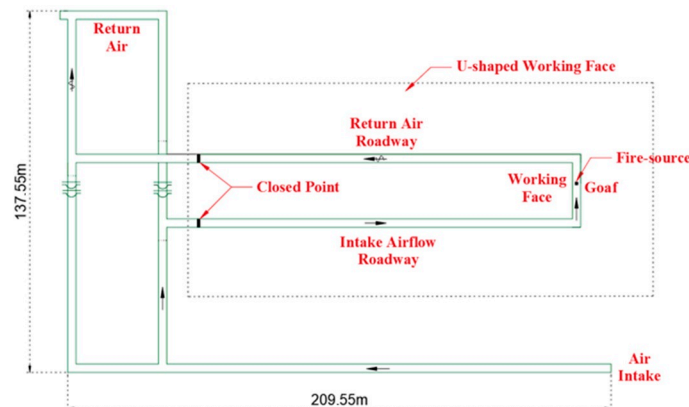


Figure 10. Schematic diagram of simulated tunnel structure: top view of road.

Firstly, we simulated the actual situation of the tunnel and used Spaceclaim software to establish a simulation tunnel model. The overall size of the model is 209.55 m × 137.55 m. It has a working face length of 21.4 m and a coal mining face conveyor and air duct length of 156.45 m. The roadway on one side of the working face air duct has a certain slope; the cross-sectional shape of the roadway is a circular arch, with a width of 3.2 meters and a height of 2.6 meters; and the fire source is set on the side of the air duct in the middle of the working face roadway, with the center of the fire source located 11.1 meters away from the outer wall of the air duct. The initial inlet air speed of the U-shaped area conveyor was set to 2.5 m/s, and the gas seepage rate was set to 0.2% of the normal ventilation rate. Gas seeped out from the working face and goaf. The simulation of the airflow field in the tunnel was simulated with the aim of achieving the gas component concentration under normal working conditions in various parts of the tunnel, and data such as the regional flow rate were obtained for subsequent simulation settings, as shown in Figure 10.

#### 4.2. Closed Simulation Settings

As for the rapid sealing process technology, a sealing sequence of “simultaneous sealing of inlet and outlet air” was adopted as the research condition. As methane accounts for over 90% of the gas component, the gas was considered methane (CH<sub>4</sub>) for the simulation research. During the sealing process, methane accumulation accelerates, causing methane to reach its explosive limit locally [28–30]. The overlap between the explosion-limited area of oxygen concentration and methane concentration in the tunnel in this simulation was considered a high-risk explosion area.

In terms of the closed speed, the change in the ventilation rate was reflected in the simulation [31]. As shown in Figure 11, the sealing process of the air bag solution was fast, the sealing was completed within 5 min, and the ventilation volume was reduced to 3% of natural ventilation. The process of sealing the gel solution involved arranging the gel bag, filling it with water to expand it so it reached the wall, allowing the ventilation volume to decrease slowly during the arrangement process, and then filling it with water until it reached the wall. This process is relatively rapid and produces ventilation. After the construction was completed, the ventilation volume was reduced to 5% of natural ventilation. The sealing process of the sea capacity plan involves laying the cement floor first. The initial layout time was long, and the ventilation volume decreased slowly during the initial layout time, and upon entering the rapid wall construction and sealing stage, the ventilation volume dropped quickly, and the time required for roof connection was longer. The ventilation volume decreased slowly, and after the construction was completed, the ventilation volume was reduced to 5% of natural ventilation.

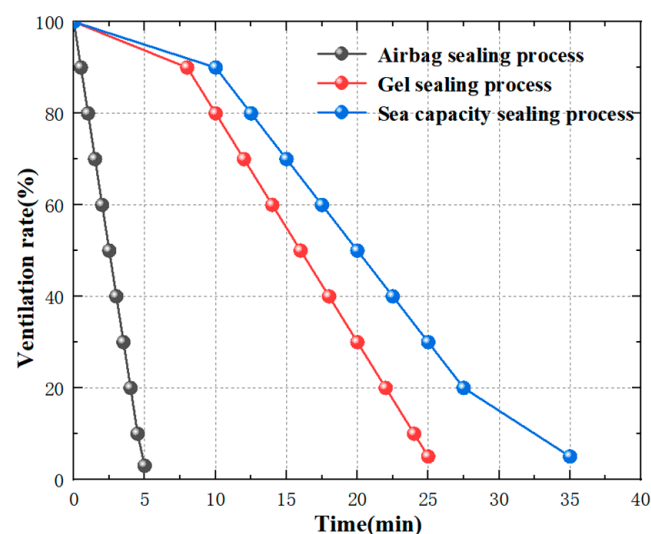


Figure 11. Changes in closed air volume under different schemes.

We set up a simulation monitoring point, with the central point of the working face roadway space as the central monitoring point, named point center. The coordinates of the central monitoring point in the model were (−1.3, 97.5, 4). Based on this point, a total of five working face roadway monitoring points, two inlet duct monitoring points, and two return duct monitoring points were established. The distribution of monitoring points in the roadway is shown in Figure 12.

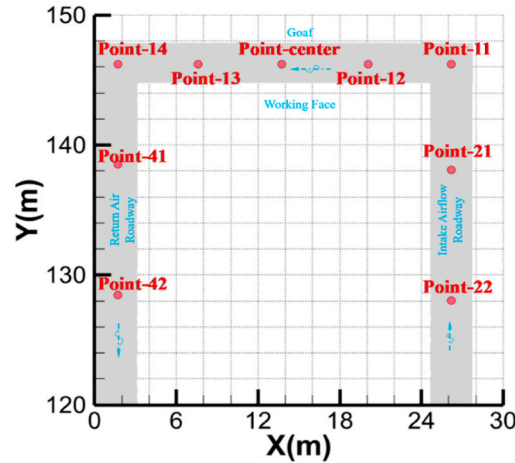


Figure 12. Partial schematic diagram of the location of model monitoring points.

### 4.3. Sealing Simulation of Ventilation System under Normal Conditions

#### 4.3.1. Simulation of Airbag Sealing Optimization Process

In this section, we describe the simulation of an initial wind speed of 2.5 m/s. The airbag completed sealing within 5 min. As shown in Figure 13, during the sealing process of the airbag, methane accumulation mainly occurred in the area near the upper corner. As the airflow continued to carry methane away, the methane concentration did not increase significantly, and the ventilation rate was gradually reduced to 3% of normal ventilation. After the sealing was completed, the methane accumulation speed became faster, but the methane concentration was still far below the explosion limit after the sealing had been completed.

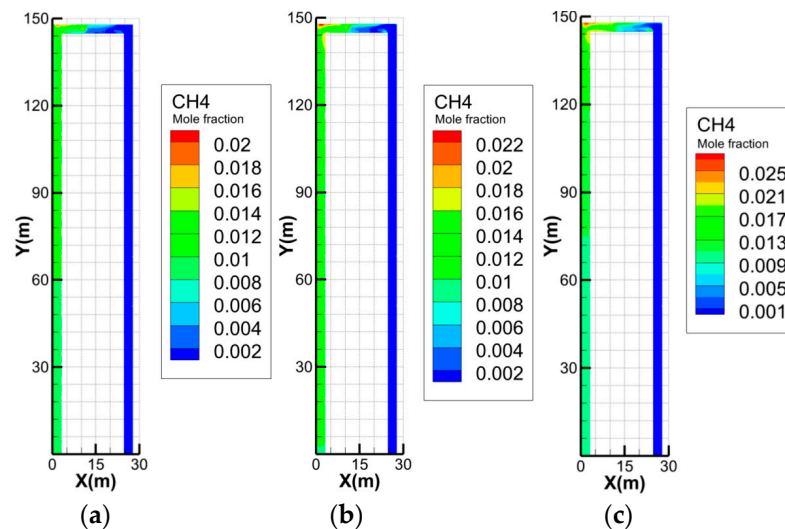
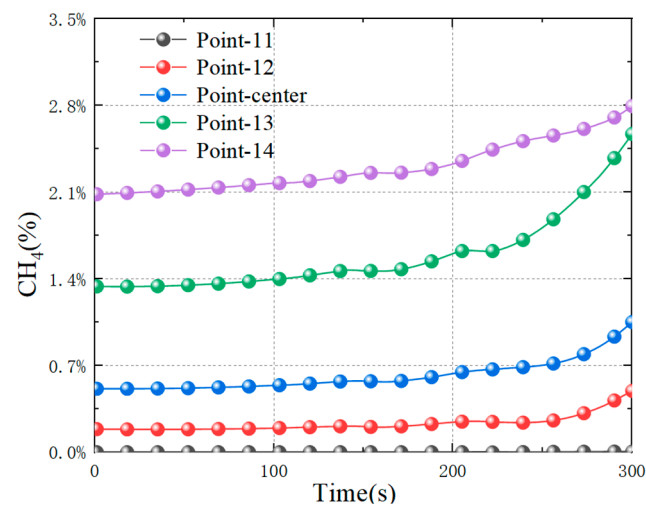


Figure 13. Changes in methane concentration during airbag sealing process: (a) 1 min; (b) 3 min; and (c) 5 min.

We selected five monitoring points, Point-11, 12, center, 13, and 14, for observation. It can be seen from Figure 14 that the CH<sub>4</sub> concentration at each monitoring point increased with time during the airbag sealing process, and the concentration growth rate became faster and faster. Among them, Point-14 was the closest to the upper corner, and the CH<sub>4</sub> concentration at this monitoring point was the highest. Generally speaking, the CH<sub>4</sub> concentration in the working face tunnel and return air tunnel rose relatively slowly, and the frequency of change was small. In the period of time before the end of the closure in 200 s–300 s, the CH<sub>4</sub> concentration increased rapidly at the monitoring points near the upper corner, including Point-13 and Point-14. At this time, methane accumulation began, and the CH<sub>4</sub> concentration in the upper corner reached a maximum of 2.8%. The methane concentration at all the monitoring points in the entire tunnel was lower than 2.8%, but it did not reach the explosion limit during the sealing process.



**Figure 14.** Methane concentration–time curve at monitoring points during airbag sealing process.

#### 4.3.2. Simulation of Closed Optimization Process of Water-Absorbing Gel

The simulated initial wind speed in this part of the experiment was 2.5 m/s, and the closure of the gel capsule was completed within 25 min. Compared with the other two optimization schemes, the sealing speed of gel was average. As shown in Figure 15, methane accumulation in the process of gel sealing also mainly occurred in the area near the upper corner. Compared with air bag sealing, the methane accumulation speed was slower, and there was no obvious accumulation in the 5th minute. In the 15th minute, although the airflow flow was large, the gas concentration still did not change much, and the gas concentration did not soar until the sealing was nearly completed.

Seven monitoring points, Point-11, 12, center, 13, 14, 41, and 42, were selected for observation. It can be seen from Figure 16 that the CH<sub>4</sub> concentration at each monitoring point increased with time during the gel sealing process, and the concentration growth rate became faster and faster. Among them, Point-14 was the closest to the upper corner, and the CH<sub>4</sub> concentration at this monitoring point was the highest. Point-41 and Point-42 were in the return air duct, and the concentration at Point-14 was not much different. The CH<sub>4</sub> concentration accumulated and increased within 1200 s–1600 s before the end of the sealing, with a sudden jump in concentration observed near the return air duct and upper corner. The CH<sub>4</sub> concentration reached 4.1%, but it did not reach the explosion limit.

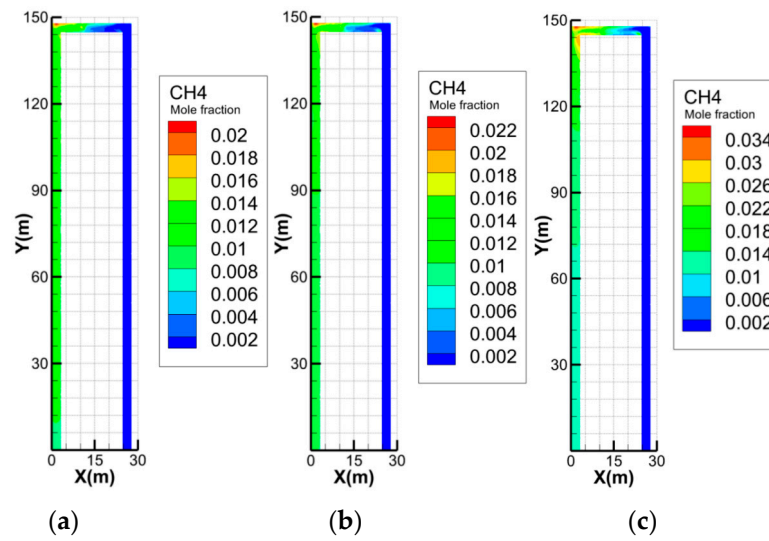


Figure 15. Change in methane concentration during sealing of gel: (a) 5 min; (b) 15 min; and (c) 25 min.

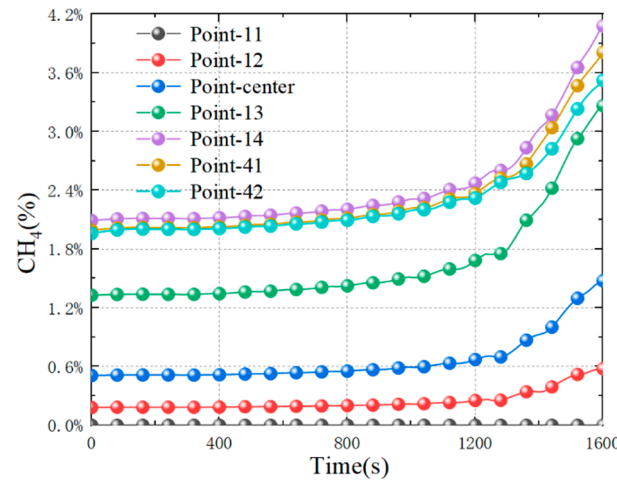
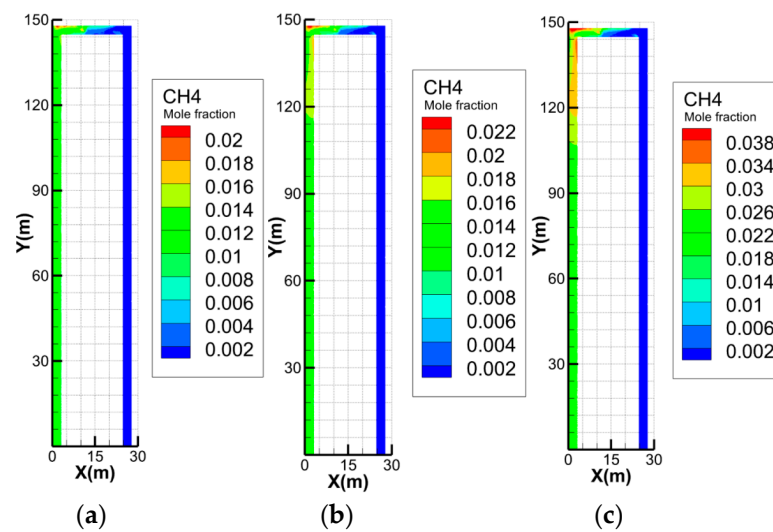


Figure 16. Time–methane concentration curve at monitoring points during sealing of gel.

#### 4.3.3. Simulation of Sealed Optimization Process for Sea Capacity Module

In this part of the experiment, we simulated an initial wind speed of 2.5 m/s and completed the sealing of the sea capacity module scheme within 35 min. Compared with the other two optimization schemes, the methane accumulation speed was the slowest and the overall time consumption was the longest. As shown in Figure 17, methane accumulation mainly occurred near the upper corner during the sealing process of the sea capacity module. At the 5th minute, there was no significant accumulation, and until the closure was completed at the 35th minute, no areas reached the explosion limit for methane concentration.

Seven monitoring points were selected for observation: Point-11, 12, center, 13, 14, 41, and 42. It can be seen from Figure 18 that the CH<sub>4</sub> concentration at each monitoring point increased with time during the sealing process of the sea capacity module, and the concentration growth rate became faster and faster. Among them, Point-14 was the closest to the upper corner, and the CH<sub>4</sub> concentration at this monitoring point was the highest. Point-41 and Point-42 were located in the air duct, with little difference in concentration compared with Point-14. It is noteworthy that compared with the first two processes, in the sea module sealing process, there was a sudden jump in methane accumulation, mainly within 100s before the end, and the value was suddenly larger. The CH<sub>4</sub> concentration near the return air duct and the upper corner was close to 4.5%, which is below the explosion limit.



**Figure 17.** Changes in methane concentration during the sealing process of the sea capacity module: (a) 5 min; (b) 20 min; and (c) 35 min.

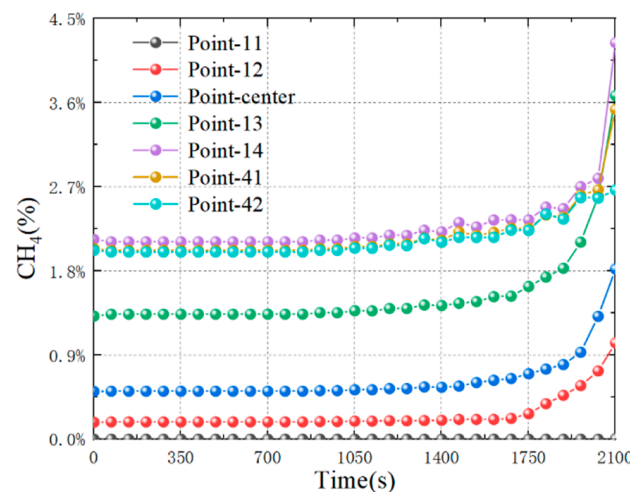


**Figure 18.** Methane concentration–time curve during the sealing process of the sea capacity module process.

Based on the numerical simulation of three processes in the scenario of “normal ventilation system in the early stage of fire”, it can be seen that setting an initial inlet air speed of 2.5 m/s provided sufficient oxygen supply to the disaster area of the working face. The CH<sub>4</sub> concentration was highest near the upper corner, and the accumulation of CH<sub>4</sub> mainly occurred in the period of time before the end of sealing. The closure of the air bag was completed in the 5th minute, and the CH<sub>4</sub> concentration reached 2.8%. The closure of the gel sealing process was completed in the 25th minute, and the CH<sub>4</sub> concentration reached 4.1%. The sea capacity module sealing process was completed in the 35th minute, and the CH<sub>4</sub> concentration reached 4.8%, which is below the explosion requirements. However, the gas concentration in the latter two processes was relatively high, especially in the closed process of the sea capacity module, being close to the explosion limit. In practice, if there is a certain airflow disturbance due to environmental factors, it will led to a certain risk of gas explosion.

#### 4.4. Closed Simulation of Ventilation System after Explosion Damage

Due to the roadway between the working face and the coal mining face having the same width, the extension length of the explosion-limited gas area in the roadway was

used as an indicator of the extension of the explosion-limited gas area. The extension length of the methane-limited area is denoted as  $L$ , and the extension length of the oxygen-limited area is denoted as  $M+N$ , as shown in the figure. The meaning of  $M$ ,  $L$ , and  $N$  in the measurement is shown in Figure 19. In this part of the experiment, we set the initial inlet air speed to 0.05 m/s to simulate the failure of the ventilation system. The effects of different sealing schemes were compared based on the extension length of the explosion-limited gas area at the end of the sealing process.

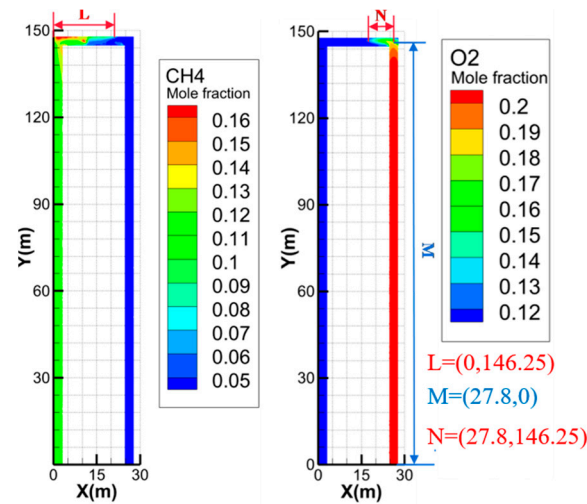


Figure 19. Schematic diagram of the extended length of the gas area with explosion limit.

#### 4.4.1. Simulation of Airbag sealing Optimization Process

The initial wind speed was set to 0.05 m/s. During the sealing process of the airbag, the faster the sealing process, the sharper the decrease in ventilation volume and the faster the methane accumulation rate, but it mainly accumulated in the working face roadway. At the same time, the diffusion of oxygen was slow, and the extension of the oxygen-limited area was slow, far from reaching the working face, without forming an explosion hazard area. At 5 min, the extension length,  $L$ , of the methane-limited gas area was 20.6 m, as shown in Figure 20a, and the extension length,  $M$ , of the oxygen-limited gas area was 10.8 m, as shown in Figure 20b.

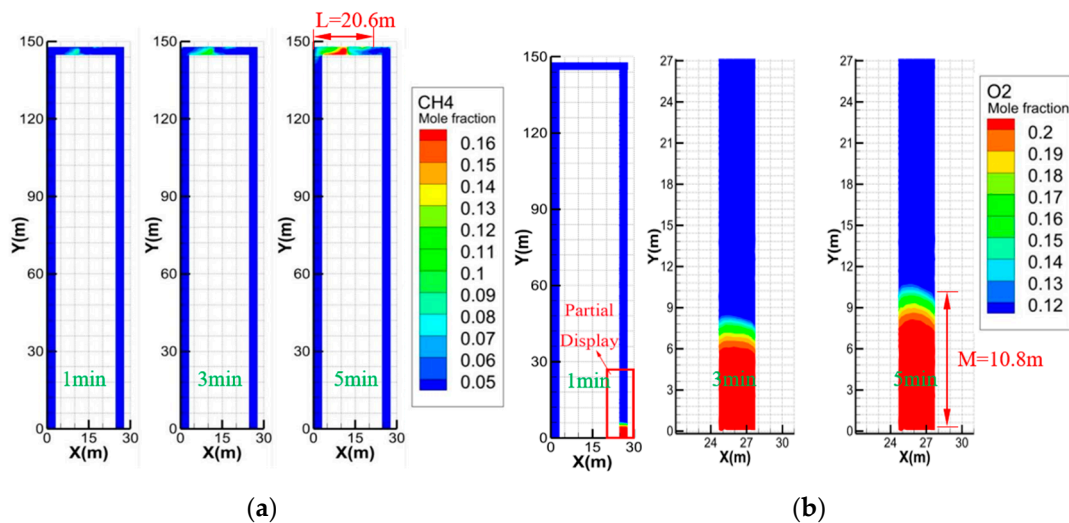
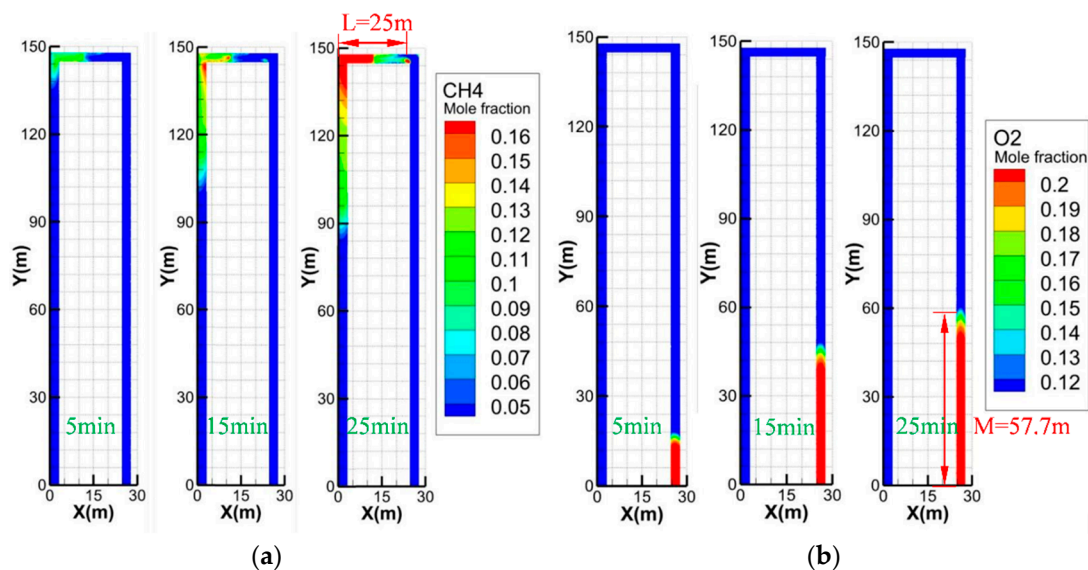


Figure 20.  $CH_4$  and  $O_2$  concentration changes during airbag sealing process after ventilation system explosion damage: (a)  $CH_4$  concentration change and (b)  $O_2$  concentration change.

#### 4.4.2. Simulation of Closed Optimization Process of Water-Absorbing gel

The initial wind speed was set to 0.05 m/s. During the sealing process of gel, the speed of sealing process was moderate, and the sealing was completed within 25 min. Methane accumulated to form a narrow accumulation zone and began to diffuse into the entry and return tunnels. Compared with the three types of sealing processes, during this process, the expansion speed of the oxygen reaching the limited area was average, it did not reach the working surface, and no explosion hazard area was formed. It was relatively safe during the construction process under the preset initial conditions. The extension length,  $L$ , of the methane-limited gas region was 25 m, and the extension length,  $M$ , of the oxygen-limited gas region was 57.7 m, as shown in Figure 21.



**Figure 21.** CH<sub>4</sub> and O<sub>2</sub> concentration changes during gel sealing after the ventilation system was damaged by an explosion: (a) CH<sub>4</sub> concentration change and (b) O<sub>2</sub> concentration change.

#### 4.4.3. Simulation of Sealed Optimization Process for Sea Capacity Module

The initial wind speed was set to 0.05 m/s. During the sealing process of the sea capacity module, the sealing process was slow, the methane accumulation speed was slow, a narrow and long accumulation zone was formed, and high-concentration methane accumulation occurred in the working face roadway and the front end of the return airway. After the sealing process was completed, the methane concentration in the return airway was relatively high. At the same time, the diffusion of oxygen was the fastest in this process among the three types of airtightness processes, and the area where the oxygen reached the limit extended faster, but it still did not reach the working surface, and no explosion hazard area was formed. It was relatively safe during the construction process under the preset initial conditions. The extension length,  $L$ , of the methane-limited gas area was 25.3 m, and the extension length,  $M$ , of the oxygen-limited gas area was 71.5 m, as shown in Figure 22.

Based on the numerical simulation of three processes in the scenario of “abnormal ventilation system in the early stage of fire”, the initial inlet wind speed was set to 0.05 m/s, and the airbag was sealed to complete tunnel sealing within 5 min. The rapid sealing process led to a sharp decrease in ventilation volume, and methane only accumulated in the working face tunnel. At the same time, oxygen diffusion was slow, and the area that reached the oxygen limit extended slowly, far from reaching the working face. During the sealing process, no explosion hazard area was formed; however, gel sealing and sea capacity module sealing were relatively slow. Due to the reduction in ventilation wind speed, methane diffused rapidly in the working face and return air roadway. Methane no longer accumulated in the working face roadway alone and began to diffuse into the inlet and return air roadway. However, no explosion hazard area was formed during

the sealing process. As the airtight construction time increased, the distance between the oxygen-limited area and the methane-limited area continually decreased. Therefore, the faster the sealing speed, the safer the construction process, and the lower the possibility of gas explosion.

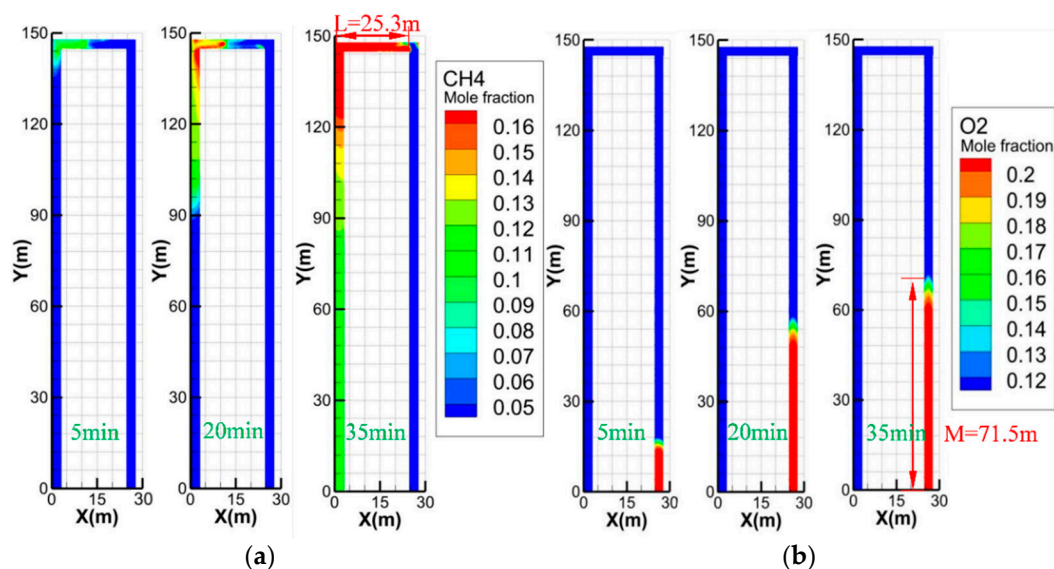


**Figure 22.** CH<sub>4</sub> and O<sub>2</sub> concentration changes during airbag sealing process after ventilation. (a) CH<sub>4</sub> concentration change, (b) O<sub>2</sub> concentration change.

## 5. Conclusions

In this research, we analyzed rapid sealing technology and processes employed in mine disasters. Based on the FAHP, three optimal sealing processes were tested, and optimization experiments were conducted for the three processes to solve the problem of sealing process defects. Using an experimental tunnel, fluent numerical simulation was used to study the dynamic characteristics of explosive hazardous gases in disaster areas. The main conclusions are as follows:

(1) By developing the Fuzzy Analytic Hierarchy Process (FAHP), conducting expert research and data collection, and the principle of maximum membership, fuzzy decision making was carried out based on fuzzy mathematical calculation. More importantly, three schemes, the sea capacity module grouting sealing process, the hydrogel material sealing process, and the air bag sealing process, were found to be the optimal schemes among all nine schemes considered in this research.

(2) According to the optimization experimental research, each of the three closed optimization schemes has its own applicable scenarios and advantages. Among them, airbag sealing requires prior deployment, which is a fast process and can achieve unmanned remote control, but the program is complex and suitable for general tunnels; the sealing speed of gel is moderate due to the restriction of a water source, but deployment personnel can leave the site early, which is suitable for tunnels with a sufficient water source; and lastly, the sealing speed of the sea capacity module is the slowest, but it has strong adaptability and is suitable for complex and irregular tunnels.

(3) When the ventilation system is normal at the initial stage of a fire, the methane concentration near the upper corner is the highest. The maximum concentration of methane during the sealing process of a closed airbag is 2.8%, the maximum concentration of methane during the sealing process of gel is 4.1%, and the maximum concentration of methane during the sealing process of a sea volume module is 4.8%, which does not meet the explosion requirements. However, the gas concentration in the latter two processes is relatively high, especially in the closed process of the sea capacity module, being close to

the explosion limit. In practice, if there is airflow disturbance, it will carry a certain risk of gas explosion.

(4) When the explosion ventilation system in the fire area was damaged, no explosion hazard area was formed during the sealing process of the three sealing processes, and the sealing effect was good. However, as the closed construction time becomes longer, the distance between the oxygen-limited area and the methane-limited area decreases, and the possibility of an explosion hazard area forming becomes higher. Therefore, the faster the sealing speed, the safer the construction process and the lower the possibility of gas explosion.

**Author Contributions:** All the authors contributed significantly to this research. F.L.: conceptualization, funding acquisition. Y.J.: conceptualization, methodology, numerical simulation, writing—original draft. C.W.: supervision, editing. B.R.: supervision and investigation. C.Z.: review, data curation. G.W.: data curation, visualization. All authors have read and agreed to the published version of the manuscript.

**Funding:** The authors are grateful for the financial support from the National Natural Science Foundation of China (52064046, 51804311), the China Scholarship Council (CSC), and the Fundamental Research Funds for the Central Universities (2023ZKPYAQ03).

**Data Availability Statement:** The data used to support the findings of this study are available from the corresponding authors upon request.

**Conflicts of Interest:** The authors declare that they have no conflict of interest.

## References

1. Yan, C. Application of Comprehensive Gas Control Technology in Fully Mechanized Mining Faces. *J. Shanxi Chem.* **2023**, *43*, 132–133, 142. (In Chinese) [[CrossRef](#)]
2. Huang, P.; Huang, W.; Zhang, Y.; Tang, S. Simulation study on sectional ventilation of long-distance high-temperature roadway in mine. *Arab. J. Geosci.* **2021**, *14*, 1674. [[CrossRef](#)]
3. Dziurzyński, W.; Krach, A.; Pałka, T. Airflow Sensitivity Assessment Based on Underground Mine Ventilation Systems Modeling. *Energies* **2017**, *10*, 1451. [[CrossRef](#)]
4. Chong, L.; Sifeng, H.; Zhijun, X. Disastrous Mechanism and Concentration Distribution of Gas Migration in Fully Mechanized Caving Stope in Wuyang Coal Mine. *Geofluids* **2021**, *2021*, 4366942. [[CrossRef](#)]
5. Gao, K.; Li, S.; Liu, Y.; Jia, J.; Wang, X. Effect of flexible obstacles on gas explosion characteristic in underground coal mine. *Process Safe. Environ. Prot.* **2021**, *149*, 362–369. [[CrossRef](#)]
6. Wen, H.; Liu, Y.; Guo, J.; Zhang, Z.; Liu, M.; Cai, G. Study on Numerical Simulation of Fire Danger Area Division in Mine Roadway. *Math Prob. Eng.* **2021**, *2021*, 6646632. [[CrossRef](#)]
7. Lei, B.; Zhao, C.; He, B.; Wu, B. A study on source identification of gas explosion in coal mines based on gas concentration. *Fuel* **2021**, *290*, 120053. [[CrossRef](#)]
8. Wang, Y.; Wen, X.; Zhang, S. Research on Key Technologies of Intelligent Quick Sealing Airbags for Mining. *Coal Min. Mach.* **2015**, *36*, 92–93. (In Chinese) [[CrossRef](#)]
9. Wen, H.; Fan, S.; Zhang, D.; Wang, W.; Guo, J.; Sun, Q. Experimental study and application of a novel foamed concrete to yield airtight walls in coal mines. *Adv. Mat. Sci. Eng.* **2018**, *2018*, 9620935. [[CrossRef](#)]
10. Hefni, M.; Hassani, F. Experimental development of a novel mine backfill material: Foam mine fill. *Minerals* **2020**, *10*, 564. [[CrossRef](#)]
11. Weiss, E.S. *Strength Characteristics and Air Leakage Determinations for Alternative Mine Seal Designs*; Department of the Interior, Bureau of Mines: Washington, DC, USA, 1993; Volume 9477US.
12. Yang, Y. Application of Roxie foam in coal mine fire prevention. *China Coal Ind.* **2015**, *3*, 64–65. (In Chinese)
13. Jin, Y.; Zhao, X.; Xiao, L.; Ren, L.; Jia, Y. The Technology of Quickly Solidifying Pulverized Coal Mortar to Construct Closed Walls. *Coal Mine Safe.* **2016**, *47*, 76–78. (In Chinese) [[CrossRef](#)]
14. Liu, S.; Ma, L.; Wei, G.; Guo, Y.; Chen, X. Study of the characteristics of fast airtight airbag in underground catastrophic wind and smoke flow. *J. China Uni. Min. Tech.* **2021**, *4*, 735–743. (In Chinese)
15. Song, X.; Wang, Z. Study on the properties of inorganic foamed concrete filling materials based on chemical foaming. *Coal Mine Modernization* **2023**, *4*, 77–81. (In Chinese) [[CrossRef](#)]
16. Luo, Z.; Deng, J.; Wen, H.; Cheng, F.; Yang, Y. Experimental study and property analysis of seal-filling hydrogel material for hermetic wall in coal mine. *J. Wuhan Uni. Tech.-Mater. Sci. Ed.* **2010**, *25*, 152–155. [[CrossRef](#)]
17. Dong, K.; Wang, J.; Liang, Z.; Shi, Q. Characteristics of CMC/ZrCit/GDL fire extinguishing gel used for mines. *China Safe. Sci. J.* **2020**, *30*, 114–120. (In Chinese)

18. Ji, L. *Application of Fast Sealing Technology in Linfen Hongda Huokou Coal Industry*; Shandong Coal Science and Technology: Jinan, China, 2019; pp. 82–83+86+89. (In Chinese)
19. Bin, Z.; Shengquan, H.; Xueqiu, H.; Le, G.; Zhenlei, L.; Dazhao, S.; Feng, S. Research on Deformation and Failure Control Technology of a Gob-Side Roadway in Close Extra-Thick Coal Seams. *Sustainability* **2022**, *14*, 11246. [[CrossRef](#)]
20. Mutton, V.; Salu, M. Full scale explosion testing and design of gypsum plaster ventilation seals. In Proceedings of the Coal Operators' Conference, Wollongong, Australia, 14–15 February 2013.
21. Gupta, S.; Kumar, U. An analytical hierarchy process (AHP)-guided decision model for underground mining method selection. *Int. J. Min. Reclam. Environ.* **2012**, *26*, 324–336. [[CrossRef](#)]
22. Xie, J.; Liu, B.; He, L.; Zhong, W.; Zhao, H.; Yang, X.; Mai, T. Quantitative Evaluation of the Adaptability of the Shield Machine Based on the Analytic Hierarchy Process (AHP) and Fuzzy Analytic Hierarchy Process (FAHP). *Adv. Civil Eng.* **2022**, *2022*, 3268150. [[CrossRef](#)]
23. Ye, H.; Chang, J. Mining Method Selection Based on Fuzzy Decision and Analytic Hierarchy Process. *J. Wuhan Uni. Tech.* **2009**, *31*, 145–148+153. (In Chinese)
24. Wang, Y.; Wen, X.; Zhang, S. Key technology research of intelligent airtight gasbag for coal mine. *Coal Mine Mach.* **2015**, *36*, 92–93. (In Chinese)
25. Liu, S.; Ma, L.; Wei, G.; Guo, Y.; Chen, X. Characteristics of Quick Sealing Airbag for Underground Catastrophic Wind and Smoke Flow. *J. China Uni. Min. Tech.* **2021**, *50*, 735–743. (In Chinese) [[CrossRef](#)]
26. Gao, K.; Yang, Z.; Yang, S.; Li, S. Study on Gas Explosion Propagation Law and Explosion Venting in an Excavation Roadway. *ACS Omega* **2023**, *8*, 5257–5273. [[CrossRef](#)]
27. Zhang, H.; Jia, Z.; Ye, Q.; Cheng, Y.; Li, S. Numerical simulation on influence of initial pressures on gas explosion propagation characteristics in roadway. *Front. Energy Res.* **2022**, *10*, 913045. [[CrossRef](#)]
28. Wang, C.; Zhao, Y.; Addai, E.K. Investigation on propagation mechanism of large scale mine gas explosions. *J. Loss Prev. Process Ind.* **2017**, *49*, 342–347. [[CrossRef](#)]
29. Xu, C.; Sun, H.; Wang, K.; Qin, L.; Guo, C.; Wen, Z. Effect of low-level roadway tunneling on gas drainage for underlying coal seam mining: Numerical analysis and field application. *Greenh. Gas. Sci. Tech.* **2021**, *11*, 780–794. [[CrossRef](#)]
30. Yu, J.; Li, Z.; Liu, Y.; Dong, Z.; Sun, Y. Regularity of Mine Gas Flow Disaster Induced by Gas Natural Ventilation Pressure after Coal and Gas Outbursts. *ACS Omega* **2021**, *6*, 19867–19875. [[CrossRef](#)]
31. Wang, G.Q.; Shi, G.Q.; Wang, Y.M.; Shen, H.Y. Numerical study on the evolution of methane explosion regions in the process of coal mine fire zone sealing. *Fuel* **2021**, *289*, 119744. [[CrossRef](#)]

**Disclaimer/Publisher's Note:** The statements, opinions and data contained in all publications are solely those of the individual author(s) and contributor(s) and not of MDPI and/or the editor(s). MDPI and/or the editor(s) disclaim responsibility for any injury to people or property resulting from any ideas, methods, instructions or products referred to in the content.